



HAL
open science

Modeling the consequences of fuel assembly bowing on PWR core neutronics using a Monte-Carlo code

Stanislas de Lambert, Guillaume Campioni, Vincent Faucher, Bertrand Leturcq, Jérôme Cardolaccia

► To cite this version:

Stanislas de Lambert, Guillaume Campioni, Vincent Faucher, Bertrand Leturcq, Jérôme Cardolaccia. Modeling the consequences of fuel assembly bowing on PWR core neutronics using a Monte-Carlo code. Annals of Nuclear Energy, 2019, 134, pp.330-341. 10.1016/j.anucene.2019.06.017 . cea-02479080

HAL Id: cea-02479080

<https://cea.hal.science/cea-02479080>

Submitted on 14 Feb 2020

HAL is a multi-disciplinary open access archive for the deposit and dissemination of scientific research documents, whether they are published or not. The documents may come from teaching and research institutions in France or abroad, or from public or private research centers.

L'archive ouverte pluridisciplinaire **HAL**, est destinée au dépôt et à la diffusion de documents scientifiques de niveau recherche, publiés ou non, émanant des établissements d'enseignement et de recherche français ou étrangers, des laboratoires publics ou privés.



Modeling the consequences of fuel assembly bowing on PWR core neutronics using a Monte-Carlo code



Stanislas de Lambert^{a,*}, Guillaume Campioni^b, Vincent Faucher^c, Bertrand Leturcq^a, Jérôme Cardolaccia^a

^a DEN-Service d'études mécaniques et thermiques (SEMT), CEA, Université Paris-Saclay, F-91191, Gif-sur-Yvette, France

^b DEN-Service d'études des réacteurs et de mathématiques appliquées (SERMA), CEA, Université Paris-Saclay, F-91191, Gif-sur-Yvette, France

^c CEA, DEN, DTN, Dir, F-13108, Saint-Paul Lez Durance, France

ARTICLE INFO

Article history:

Received 21 January 2019

Received in revised form 6 June 2019

Accepted 8 June 2019

Available online 21 June 2019

Keywords:

PWR

Monte Carlo

Modeling

Bowing

Tripoli-4[®]

ABSTRACT

The effect of assemblies bowing in PWR nuclear reactors onto core neutronics is an observed phenomenon still poorly understood which can lead to Power Ratio Tilt. Studies of the consequences of rod/assembly bowing involve many different fields addressed by nuclear power plant, such as neutronics, thermohydraulics, mechanics... in a complex combination of multi-physical interactions. For the neutronic part, the modeling of bowed assemblies in Monte Carlo codes must allow to correctly describe the shape of fuel rods. In this article, two discrete ways to model bowed geometries are tested: the first one consists in a stacking of vertical small cylinders following the shape of the fuel rod by small shifts between neighboring cylinders; the second one, newly introduced in the present research, consists in a sequence of rotated cylindrical segments arranged to as to follow the shape of the fuel rod more closely. Both models are used to reproduce two specific bowing patterns, namely C-shape and S-shape, for which a reference modeling involving an analytical toroidal volume cut by planes is available for use with CEA's Monte Carlo code Tripoli-4[®]. Results of comparisons between both models and analytical reference show that, even if the segment modeling requires a specific effort to handle implementation constraints, it appears preferable compared to stacking modeling. It provides accuracy with fewer discrete entities and is therefore computationally affordable and it is far more robust when increasing bowing deflection. This approach is thus only considered ready for its application to any kind of bowing patterns.

© 2019 Elsevier Ltd. All rights reserved.

1. Introduction context and problematics

The present paper aims at contributing to the analysis of the interaction between Fuel Assembly bowing and Power Distribution for Pressurized Water Reactors. It notably addresses a common issue known as Power Tilt (Andersson, 2005; Kerkar and Paulin, 2008; Grard, 2014), corresponding to a static azimuthal dissymmetry of the power distribution in the reactor core. It may occur even from the very start of the reactor (i.e. with a new set of fuel assemblies) with characteristics apparently connected to the specific technology of one given type of reactors (Grard, 2014) (i.e. French 900 MW PWR or 1300 MW PWR for instance).

Even though the Tilt phenomenon is clearly defined and measured (thanks to the Quadrant Power Tilt Ratio) (Saeed, 2016; Kerkar and Paulin, 2008), it results however from a complex combination of multi-physical interactions, involving for instance thermohydraulic variations (density and temperature of the coolant),

fuel assembly handling and mechanics, coolant pump start-up sequence, imbalance of the flow between the main loops of the primary circuit, or of the extracted thermal power between the different steam generators (Grard, 2014; Gabrielsson, 2018; Andersson, 2005). It can affect the power management strategy of the concerned reactors, leading to strategic and rather confidential material out of the scope of the proposed research. On the contrary, we propose to investigate one of the couplings introduced above known to be of primary importance (see for example (Grard, 2014) or (Kerkar and Paulin, 2008) for general information about supporting this statement), to provide some methodological knowledge on how it develops and evolves, as well as some solutions to model it with accuracy and efficiency.

The addressed coupling is thus the link between power distribution and bowing of fuel assemblies and the paper is organized as follows. First, the mechanical characteristics of a PWR fuel assembly are recalled, as well as the way its deformation affects neutronics in its vicinity. On the one hand, it directly modifies the geometric configuration of the medium where the population of neutrons evolves, and on the other hand, it indirectly modifies

* Corresponding author.

E-mail address: stanislas.de-lambert@cea.fr (S. de Lambert).

some thermalhydraulic quantities through the local redistribution of the flow (such as fluid temperature or density). The latter phenomenon being notoriously complex and the subject of extensive ongoing research in hydrodynamics, it is handled only through simple models in the present paper, to mainly provide basic sensitivity results. The second chapter is specifically dedicated to the introduction of the description of a bowed fuel assembly in a Monte-Carlo model for neutronics and to the comparison between different modeling strategies in terms of accuracy and computational efficiency. Some well-chosen configurations are then studied in the third, fourth and fifth chapters to illustrate the potential of the coupled system previously built and to give some insights on the relative influence of coupling parameters.

2. Short review of the impact of assembly bowing of neutronics

2.1. Interest for taking fuel assembly bowing into account within neutronic analyses

Assembly bowing has been first observed in a nuclear core following RCCA (Rod Cluster Control Assembly) insertion issues (IAEA, 2008) in the early 1990s (see for instance an example of bowed assembly in Fig. 1 and pieces of available public knowledge information in Fig. 2). Neutronic modeling of bowing has then received much attention, because of several significant consequences. Those include fuel cycle management (Li, 2017a,b), ex-core instrumentation (Konheiser, 2016), safety regarding departure from nucleate boiling (Mukin, 2017; Mukin, 2018), rod design evolution (Fetterman, 2008) (since neutronic effect also has in return an actual impact on mechanics, see for instance (Karlsson, 1999; Syrjälähti, 2019)), and more generally core management policies (Kerker and Paulin, 2008). The range of deformation can lead to 20 mm water gaps within the core (Shishkov, 2015; IAEA, 2008; Fetterman, 2008), representing a reference value used further to validate the proposed models. In (Konheiser, 2016), the author considers a maximal deflection of 1 cm, leading to water gap openings of the same order of magnitude. Fuel assembly bowing patterns are also known to be classically C-shaped, or S-shaped (IAEA, 2008; Gabrielsson, 2018; Andersson, 2005) – named respectively first order and second order deformation patterns later –, and in certain cases, calculations have shown that assemblies could undergo W-shaped deformations (Wanninger, 2018). Obviously, actual in-core assembly bowings are not ideal, in the sense that they are not literally C-shaped, S-shaped or even W-shaped. The



Fig. 1. View of a PWR bowed fuel assembly (Fernandez, 2010).

first two patterns are nonetheless representative enough to provide the necessary evaluation of the proposed modeling strategy, built to handle thereafter any kind of deformations.

2.2. Monte-Carlo modeling of rod/assembly bowing

Monte-Carlo method is a stochastic way of simulating neutronics. It does not require meshing since equations of geometric surfaces are directly taken into account. Almost any geometry can be very accurately handled, yielding generally rather computationally demanding simulations, standing as reference solutions for complex situations. Monte-Carlo results are also classically used to validate deterministic meshed methods to be used for engineering purposes. This method has recently shown its reliability to model a PWR fuel assembly for parametric studies (Kępiński, 2016).

Recent developments in 2D Monte-Carlo simulation (core mid-plane) to consider bowing consists in shifting one entire rod horizontally from its initial pin cell position. For instance, in (Li, 2017a), authors consider a 3×3 pin cell lattice with SERPENT-2 (Serpent, 2015), and shift the central rod to simulate a deformation, in (Mukin, 2018) they consider a 7×7 pin cell lattice (also with SERPENT) and also shift the central rod. This action implicitly changes the moderating volume. The method remains similar at the scale of an assembly, considering a 3×3 lattice of assemblies, and shifting the central one (Shishkov, 2015; Li, 2017b).

A recently presented 3D model divides the rod bowing in several cylindrical layers (Li, 2017a), and then shifts the layers independently to simulate a C-shaped deformation, demonstrating the feasibility of simulating 3D deformations with SERPENT-2 (Serpent, 2015). This model is then used latter in a 3×3 assembly lattice (the assembly in the middle is made of 3D C-shaped rods), in a second article from the same author (Li, 2017b). Even though this is not directly the topic of the paper, a deterministic approach of assembly bowing is also presented in (Li, 2017b).

To contribute on this topic, the next chapter thus describes two Monte-Carlo 3D-models of one single fuel rod implementing approximate discrete representation of the rod. The first model (called stacking, see below) is very similar to the one used in (Li, 2017a), to connect with the identified state-of-the-art, while the second model is a new approach specific to the current article. The obtained results for both models are compared and discussed using a comparison with a reference solution based on an exact geometric representation of the deformed rod available only for pure analytical C- or S-shape bowing. Upscaling from the rod to the fuel assembly is also considered, provided well-chosen hypotheses.

Finally, all the simulations in this paper are performed using Tripoli-4[®] software (Brun, 2015), developed at CEA. The cross sections library used is JEFF3.1.1 (Santamarina et al., 2009). All simulations are normalized to one emitted neutron ($k_{\text{eff}} = \text{production rate}$).

3. Efficient and accurate model of fuel assembly bowing for a Monte-Carlo neutronic solver

3.1. Modeling framework for rods and assemblies

In terms of modeling of structures, Tripoli-4[®] software, and more generally classical Monte-Carlo simulation programs for neutronics, allows modeling a large number of 3D geometries through analytical shapes. A combination of toroidal shapes can be used to represent typical first order and second order bowing shapes of the rods, as illustrated in Fig. 3, but this comes with a significant computational cost of the associated simulations due the numerical overhead of geometrical operations involving toroid structures

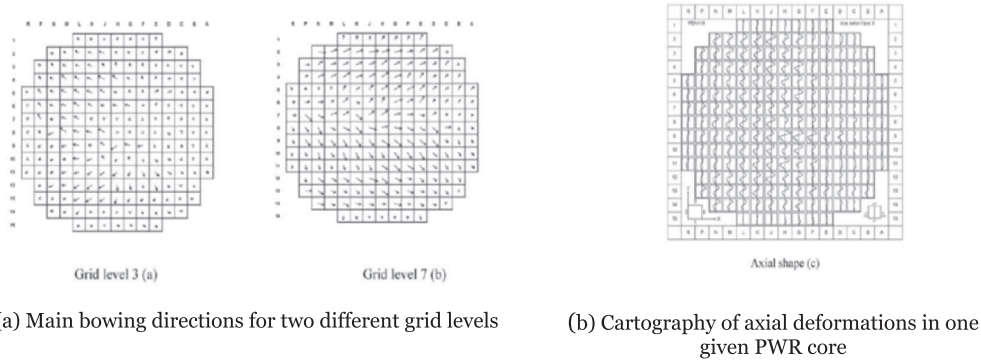


Fig. 2. Public domain information about fuel assembly bowing and axial deformation (AIEA, 2010).

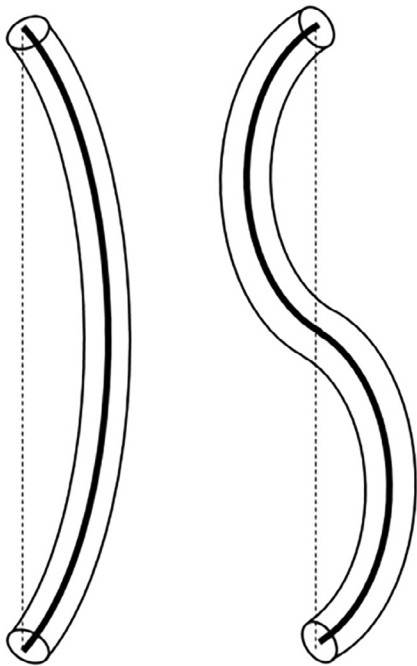


Fig. 3. Typical first order (left) and second order (right) deformed shape of a fuel rod (represented as an equivalent beam for the sake of simplicity, with neutral fiber displayed in thick black line).

compared to classical shapes, especially when dealing with partial or complete assembly(ies) composed of numerous rods.

Moreover, this strategy reaches a limit when considering the generic deformation of an assembly with no analytical expression usually available in MC codes. This justifies the need for alternative semi-discrete approaches able to handle any kind of transverse displacement along the rod, as stated in the Section 2.3. The idealized first order and second order bowing shapes in Fig. 3 are yet of primary interest since they are compatible with Tripoli-4[®] modeler and thus provide valuable reference solutions to evaluate the capabilities of the proposed extended modeling approaches.

The characteristics of a deformed rod are deduced from the reference properties of a straight rod using the following set of basic hypotheses, derived from the Small Perturbation hypothesis, fully applicable with maximal deflection of 1 cm along ~4 m long rods (see (Patarin, 2002) for some general elements about PWR fuel assembly design):

1. The section of the deformed rod remains circular with a constant radius along the rod equal to the radius of the straight rod and orthogonal to the neutral fiber.

2. Under Hypothesis 1, the conservation of the total mass of the rod and of the density of the material yields the conservation of the volume between straight and deformed rod, and thus the conservation of the length of the neutral axis of the rod (as illustrated in Fig. 4).

Practically, given a classical parametrization of the neutral fiber as a function \mathbf{f} (scalar function for plane strains or vector function with 2 components for generic 3D strains) of the vertical coordinate z , Hypothesis 2 writes:

$$\int_{z_0}^{z_1} \sqrt{1 + \|\nabla \mathbf{f}\|^2} dz = H \quad (1)$$

where z_0 and z_1 are the altitudes of the lower and upper ends of the rod respectively, H is the height of the straight rod.

Finally, for further work involving a partial or complete fuel assembly built from a series of rods, it would be additionally assumed that all the rods have the same deformed shapes, corresponding to the global shape of the assembly, so that the results in the present article directly apply. This rather classical hypothesis is supported by the presence of several grids along the assembly, acting as spacers and keeping the pitch of the rod lattice constant (see again (Patarin, 2002)).

3.2. Representation of deformed rods

3.2.1. Toroidal reference model

It corresponds to a simple arc shape, whose maximal deflection is given at mid-height. It is represented by a full torus (in black in Fig. 5) cut by two planes (in green), so that the length of the resulting torus section is equal to the length of the straight rod.

3.2.2. First alternative modeling derived from the work of Li et al.: stacking modeling

Stacking modeling, illustrated in Fig. 6 is geometrically rather simple. It consists in “stacking” small vertical cylinders with their centroids located on the neutral fiber of the deformed rod.

The advantage of such a method comes from the set of non-overlapping cylinders, all vertically oriented: the quantity of fuel in the straight rod is thus natively preserved. In return, the association of vertically oriented cylinders exhibits the following drawbacks:

1. some severe discontinuities in the description of the rod can occur if too few cylinders are used in the area of maximal slope of the deformed rod introducing some important gaps in its modeling; this can result in side effects regarding the global influence of the rod onto neutronics,

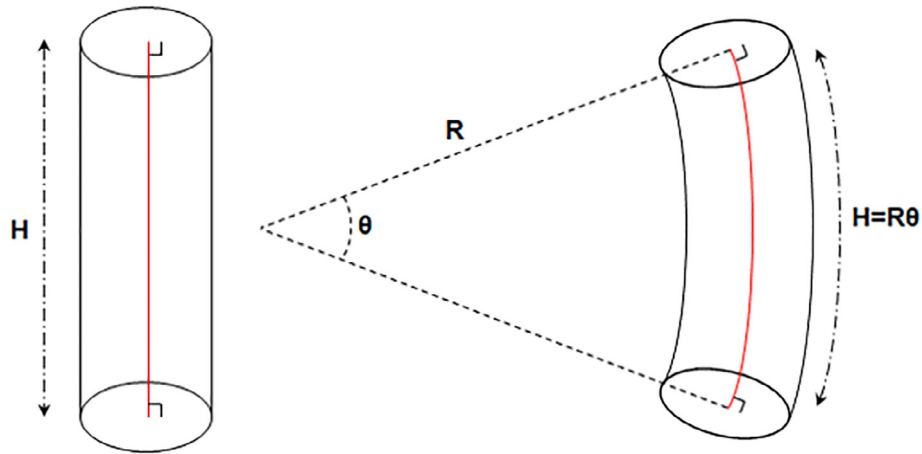


Fig. 4. Conservation of the length of the neutral fiber of the rod (in red) between the straight rod on the left and the deformed rod of the right.

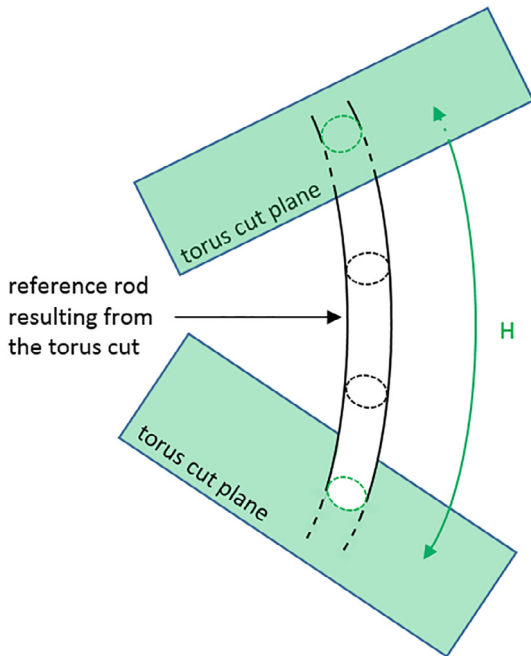


Fig. 5. Illustration of the toroidal reference model.

2. the total height of the cylinders and the actual length H of the rod are not equal, as the sum of the axial lengths of the cylinders is equal to the distance z_1-z_2 between both ends of the deformed rod, without taking its curvature into account, i.e., starting from Eq. (1):

$$\sum_{i=1}^{\text{Number of cylinder}} h_i = z_1 - z_2 \neq H \quad (2)$$

One potential way to circumvent this last issue, especially for significantly bowed rods where it could alter the physical solution, is to introduce two “corrective” cylinders of very low height at the top and bottom of the stack to retrieve the right length of the rod (as shown in Fig. 6).

3.2.3. New alternative modeling for generic deformed shape: segments modeling

This method models any deformation by discretizing the rod into small rotated cylindrical segments oriented according to the local curvature of the deformed rod, as illustrated in Fig. 7.

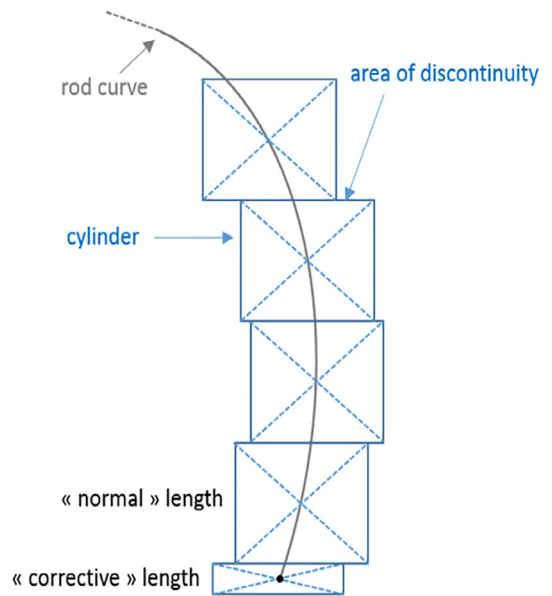


Fig. 6. Stacking modeling with corrective length to ensure total length conservation.

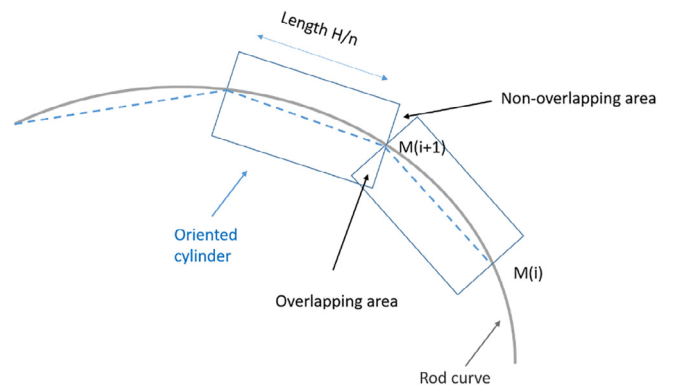


Fig. 7. Illustration of segments modeling accounting for actual rod curvature.

The discretization in segments consists in cutting the curve of the deformed rod into small inclined cylinders called “segments”, of axial length H/n , where H is the total length of the rod and n the number of segments of the discretization.

This representation defines implicitly a set of points $M(i)$ corresponding to the intersection of cylinder axis with the neutral fiber of the rod, so that a segment can be identified from the couple $[M(i), M(i+1)]$. The orientation of Segment $[M(i), M(i+1)]$ is then obtained from the string between points $M(i)$ and $M(i+1)$ and the length is much more accurately conserved, with a linear convergence towards the exact conservation with respect to the number of segments.

The proposed method yet exhibits some specific issues to be handled carefully to perform robust and accurate Monte-Carlo simulations:

1. segment cylinders are overlapping each other (see overlapping areas in Fig. 7) in the general case due to inclination, which requires to give priority to one segment over another,
2. the corollary of these overlapping zones is the existence of gaps (called “non-overlapping” areas in Fig. 7) which causes a violation of the conservation of the amount of fuel in the rod provided the segment cylinder radius equals the rod radius.

These issues are solved by the following modeling guidelines:

1. always use an odd number of segments,
2. adjust the length of the segments with even identification numbers (id) to fill the spurious gaps as illustrated in Fig. 8,
3. within the Monte-Carlo solver, give priority to the segments with odd id over the segments with even id to cancel the potential overlapping conflicts.

The length correction, denoted ε , for each segment can be deduced from a visualization of the default segment model built using the string lengths measured along the rod neutral fiber (for instance using T4G viewer of Tripoli-4[®]). It can also be computed in a preprocessing step from the initial length of the segment and the local curvature of the rod (however not implemented in this preliminary research). In the following paragraphs, the value of the correction is estimated for a maximal deflection of 20 mm and a number of 51 segments, and kept constant for all configurations, with no visible side effects thanks to the priority established within the segments.

3.2.4. Building computational models from actual assembly bowing data

This last paragraph aims at concluding the current section dedicated to modeling strategies by giving some insights for processing industrial bowing data and building of relevant and accurate

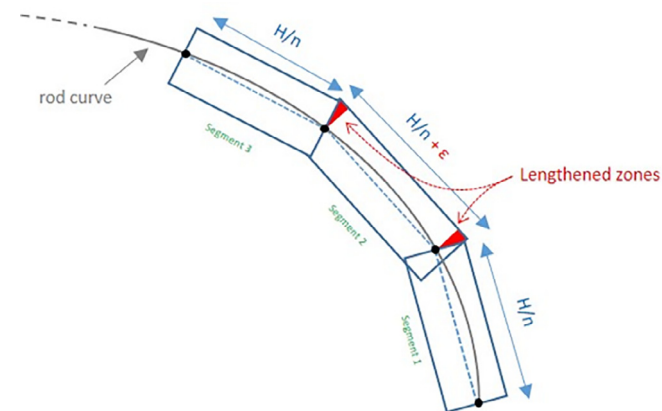


Fig. 8. Length correction to keep mass quantity, with segment 2 lengthened to close non-overlapping areas.

models taking them into account. Three engineering steps have thus to be considered.

First, bowing measures, obtained on-site in an actual plant after core unloading for instance, provide the deflection of the full assembly at a discrete number of locations along its main axis. If this number is in accordance with the targeted number of discrete items used to describe one modeled rod, they can be used directly to position the centroids of the stacked cylinders or the approximating segments accordingly. Otherwise, a reconstruction of the shape of the assembly from the discrete data is necessary.

This second step can be seen either from a purely mathematic point of view or from a mechanical one. Mathematically, it consists in choosing an interpolation function for the neutral fiber (the same for the assembly or the rods). When using polynomial functions, the order of the function is logically adjusted to the dominant shape observed in the original data, if any, resorting for instance to the basic classification provided in Section 2.1. An alternative strategy is to deduce the shape of the assembly from a direct mechanical computation using a beam model for the assembly and introducing the measures as imposed displacements. In this case, a Timoshenko beam model is the most relevant choice, since the assembly can undergo large levels of shearing, and some constraints can be added to increase the fidelity to the industrial device. For instance, the curvature of the beam can be forced to zero at the grid levels to account for their effect as spacers in the assembly.

The final step consists in automatically generating the datasets for Monte-Carlo simulation from the geometrical data reconstructed above.

The complete automated process implemented in the current paper is illustrated below for the significant case of a central symmetric second order analytical shape of the rod (see Fig. 9).

The global deflection x is approximated along the vertical direction z through the polynomial expression:

$$f(z) = az + cz^3 \quad (3)$$

With the set of coefficients given by:

$$\begin{cases} \frac{df}{dz}(z_m) = 0 \\ f(z_m) = -f_m \end{cases}, \text{ yielding : } a = -\frac{3f_m}{2z_m}, c = \frac{f_m}{2z_m^3} \quad (4)$$

Given the global shape of the neutral fiber of the rod, Hypothesis 2 provides the value for extremum vertical coordinates z_0 through the solution of the non-linear equation:

$$\int_{-z_0}^{z_0} \sqrt{1 + \left(-\frac{3f_m}{2z_m} + \frac{3f_m z^2}{2z_m^3}\right)^2} dz = H \quad (5)$$

Eq. (5) can be solved analytically using Formal Calculus software or in closed form. Once the reference shape of the rod is completely defined, segments are automatically generated taking into account the guidelines expressed in the previous paragraph. The model built from the conditions above is shown in Fig. 10, with significant shrinkage along the vertical axis for illustration purposes (as stated in Section 3.1, H is classically close to 4 m, for maximum deflection around 10 mm).

4. Compared results for first order rod deformation

The comparison is carried out in the case of French PWR 900 MW geometry. The length of the rods is thus $H = 3.658$ m, with a lattice pitch of $p = 1.26$ cm, and a fuel rod diameter of $d = 9.5$ mm. The considered physical situation is given in Fig. 11 and views of the computational models are given in Fig. 12, with maximal deflections of $\lambda = 10$ mm, 20 mm and 25 mm. We define $\alpha = p-d$. This situation illustrates an external bowed fuel rod with an

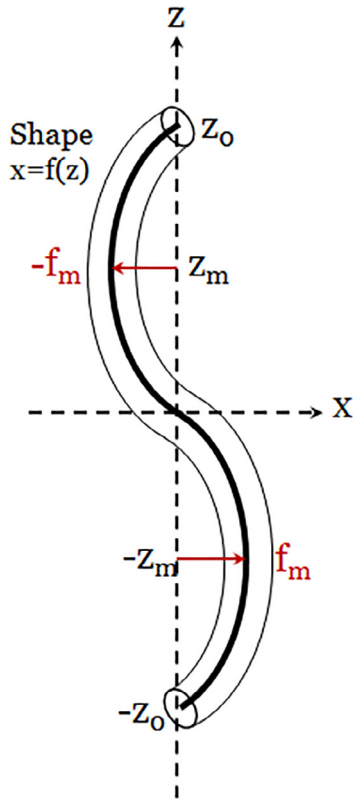


Fig. 9. Typical central symmetric second order shape of the neutral fiber with two maximal deflection points at respective coordinates $(f_m, -z_m)$ and $(z_m, -f_m)$.

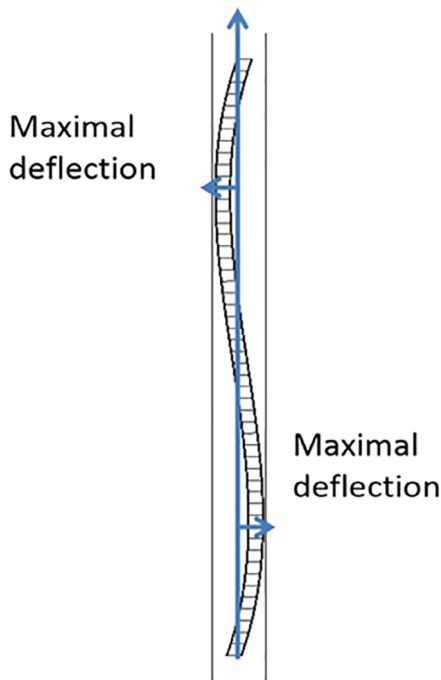


Fig. 10. Illustration of Tripoli-4[®] modeling through segments for planar symmetric second order rod deformation (vertically shrunk view stemmed from T4G viewer).

increased water gap on the left and a fuel rod row on the right (following the same deflection). The neutron sources are distributed in the fuel volume inside the rod and neutrons are generated following a Watt fission spectrum. A maximum of 100 000 batches (20

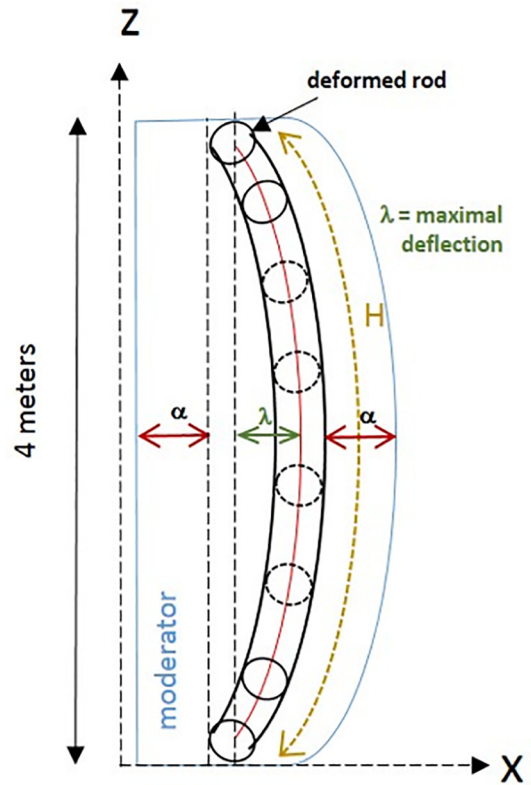


Fig. 11. Considered geometry and boundary conditions for the first order comparison case (lateral, top and bottom boundaries are set to reflection, Y-axis boundaries are set to translation).

discarded) of 10 000 particles has been set up for all simulations. We consider that all batches are widely independent.

The toroidal analytical model provides the reference solution against which the semi-discrete approaches (stacking and segments) are confronted. For the stacking or segment approaches, various numbers of discrete entities are considered, from 20 to 550 stacked cylinders and from 21 to 101 segments respectively. For the latter modeling, the length correction is computed once for the case with 51 segments and applied to all other configurations with commented results whenever necessary.

Selected quantities of interest for the assessment of the various models are neutron production rate in Uranium 235 (U-5), neutron absorption rate in Uranium 238 (U-8) and global k_{eff} coefficient for the chosen configuration. Conditions are close to a French 900 MW start: no previous irradiation, fuel in new condition, boric acid concentration of 1440 ppm, a 5% U-5 enrichment (see (Kerker and Paulin, 2008; Coppolani, 2004) for general statements about French PWRs). 3σ -error bars are associated in following graphics to all quantities resulting from Monte-Carlo statistics. It is noticeable that all performed simulations involved the same number of emitted neutrons. Deviations from the reference obtained with the toroidal model therefore derive only from differences in reaction rates.

Detailed results are given in the next two paragraphs for the 20 mm-deflection situation, whereas results for all deflections are compiled in Section 4.3.

Remark 1: Adjusting vertical and horizontal scales in Fig. 12 (and identically in Fig. 19) logically results in some distortions of the elementary shapes implemented in the reference model and in the segment model. The torus does not appear as such due to the apparent modification of the angle between the extremum

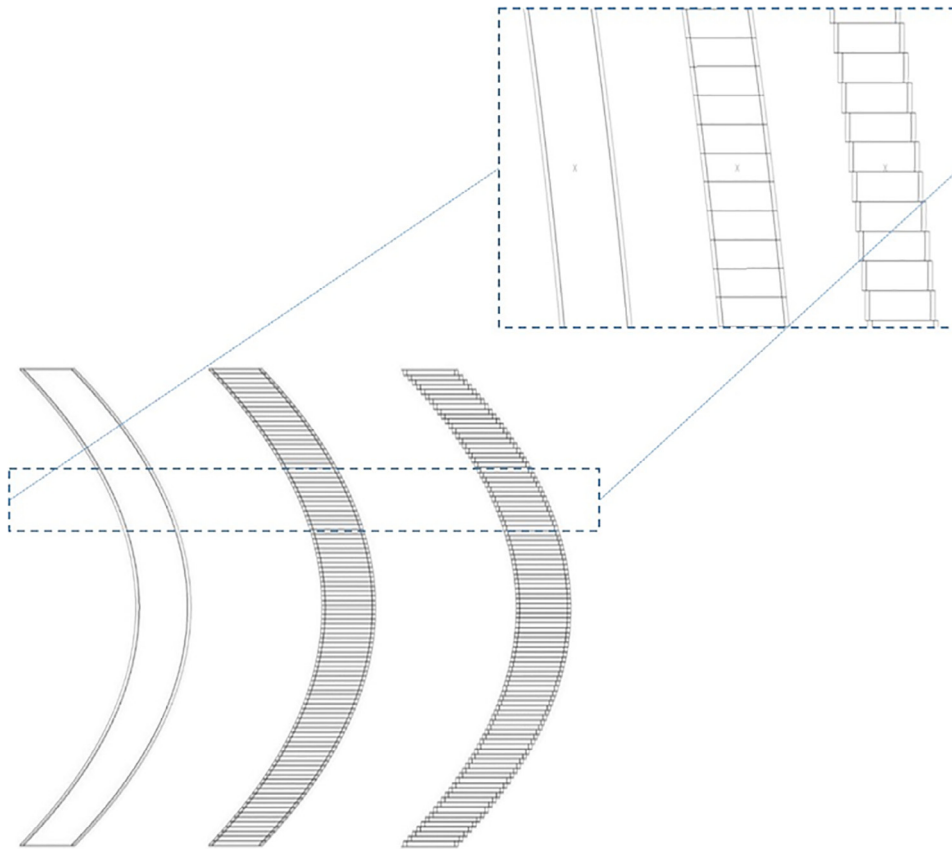


Fig. 12. Illustration of computational models for first order deformation, with distinction between the inner part of the rod with fuel properties and the lateral part with cladding properties (from left to right: cut torus (reference), segments, and stacking, scales not conserved for the sake of clarity). The fuel-clad gap is too small to be observed on the figure.

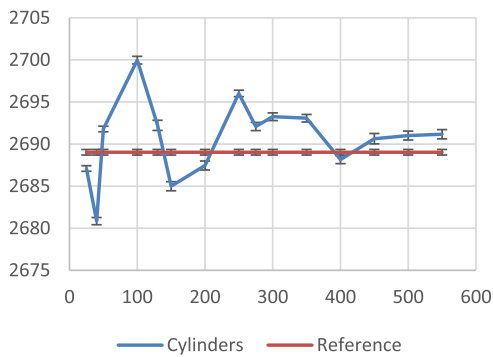
sections and the neutral fiber, and 2D-projections of segments are transformed from rectangles into parallelograms. These visual artifacts do not affect the purpose of the proposed view, which is to highlight the major differences between the semi-discrete approaches and the reference, especially close to the interfaces between discrete entities.

Remark 2.: There would be no relevance in comparing the results presented below to results from a close configuration implementing a straight rod. The proposed test case is designed to compare the modeling approaches. The solution is greatly influenced by the arbitrarily chosen boundary conditions, with a fuel/moderator

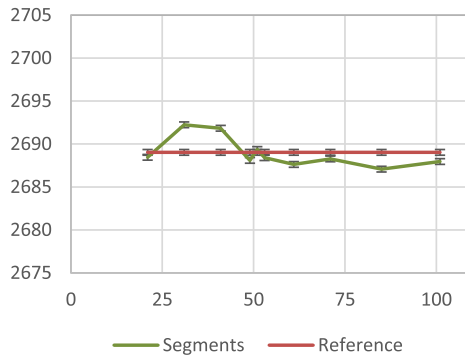
ratio given by the global geometry of the computational domain, so that the actual value of the multiplication factor is physically meaningless. The foreseen comparisons shall be performed in further research through the proper modeling of a partial or complete nuclear core configuration implementing potential bowing of some fuel assemblies.

4.1. Neutrons production and absorption rates

Results for neutron production in U-5 are provided in Fig. 13, whereas results for neutron absorption in U-8 are provided in Fig. 14.

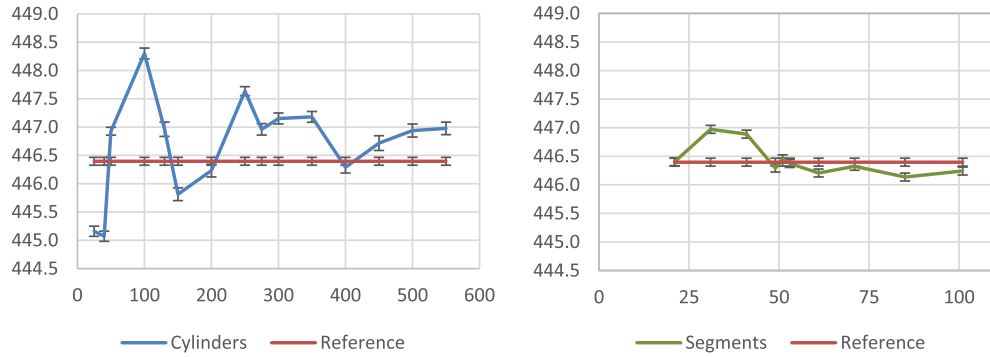


(a) Production rate (s⁻¹) obtained with stacking modeling implementing 20 to 550 cylinders



(b) Production rate (s⁻¹) obtained with segment modeling implementing 21 to 101 segments

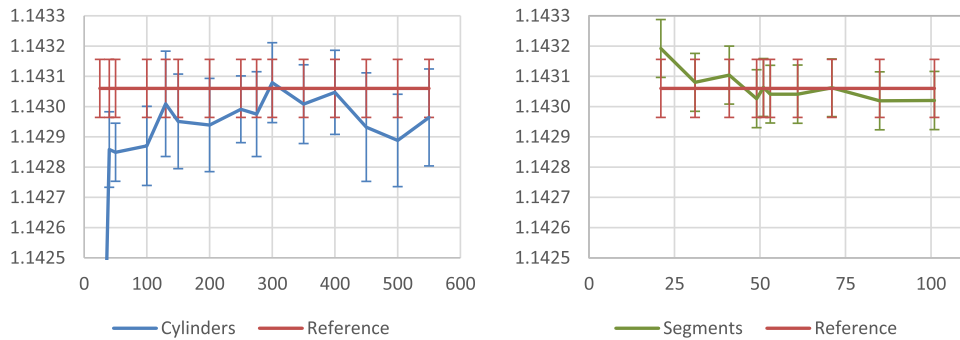
Fig. 13. Neutron production rate in U-5 for stacking and segment modeling compared to reference.



(a) Absorption rate (s^{-1}) obtained with stacking modeling implementing 20 to 550 cylinders

(b) Absorption rate (s^{-1}) obtained with segment modeling implementing 21 to 101 segments

Fig. 14. Neutron absorption rate in U-8 for stacking and segment modeling compared to reference.



(a) k_{eff} obtained with stacking modeling implementing 20 to 550 cylinders

(b) k_{eff} obtained with segment modeling implementing 21 to 101 segments

Fig. 15. k_{eff} coefficient for stacking and segment modeling compared to reference.

The segment modeling generally yields results much closer to the reference than the stacking modeling. The influence of the geometric correction is clearly visible, since the simulation with 51 segments (for which the actual correction is computed) are the most accurate, with a slow discrepancy appearing for higher numbers of segments despite the better approximation of the rod curvature.

As far as stacking modeling is concerned, the configuration with 400 cylinders provides accurate results, but the accuracy decreases again for higher numbers of cylinders, with no obvious explanation contrary to the case of segment modeling (see Section 4.3 for further analysis).

4.2. Global k_{eff} coefficient

If previous results provided insights about the proximity of behavior of the semi-discrete models compared to the reference, results in terms of k_{eff} coefficient have priority to actually evaluate their accuracy. They are given in Fig. 15.

Results obtained with segment modeling are again closer to the reference than those obtained with stacking modeling. It is noticeable that the latter seems to systematically underestimate the rod reactivity which could prove to be an issue when dealing with safety evaluations. Some fairly accurate results are yet observed for some high number of stacked cylinders (around 300) but they are difficult to predict and lack robustness since higher numbers can still produce large deviations. Taking into account that the computational cost of stacked cylinders is close to that of segments

for the same number of elements (see Fig. 16), it demonstrates that segment modeling with the guidelines proposed in Section 3.2.3 should definitely be preferred to represent the bowed fuel rod in the present configuration (more accurate, with less elements).

Looking deeper into segment modeling, the range of segment numbers producing accurate results is quite wide (from 51 to 71). Smaller numbers should be avoided, with a significant increase of the deviation from the reference when going down towards 21 segments. Higher numbers around 100 segments do not show the expected accuracy, which can be imputed to the length correction which should be specifically computed for these configurations. Anyway, trying to retrieve some accuracy with high

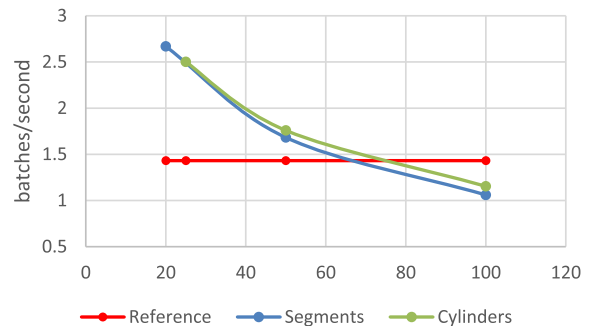


Fig. 16. Computational performance in terms of batches per second, for segment and stacking modeling and reference toroidal modeling.

Table 1
Compiled results for both semi-discrete approaches and three values of deflections (10, 20 and 25 mm): deviation for production rate (in %), absorption rate (in %) and k_{eff} coefficient (in pcm). For rates: $\sigma < 0.1\%$ and for $k_{\text{eff}} \sigma < 15$ pcm σ .

	Deflection	Segment			Stacking		
		Deviation			Deviation		
		Min	Mean	Max	Min	Mean	Max
U5 (%)	10	0,02	0,05	0,10	0,01	0,07	0,21
	20	0,01	0,05	0,12	0,08	0,21	0,41
	25	0,01	0,03	0,07	0,01	0,11	0,27
U8 (%)	10	0,00	0,03	0,08	0,00	0,07	0,21
	20	0,01	0,05	0,13	0,03	0,22	0,43
	25	0,01	0,04	0,08	0,02	0,13	0,24
K_{eff} (pcm)	10	6,90	10,57	16,40	0,70	5,38	13,10
	20	0,20	2,47	4,40	14,00	20,73	35,60
	25	0,40	3,80	6,20	0,80	17,40	37,90

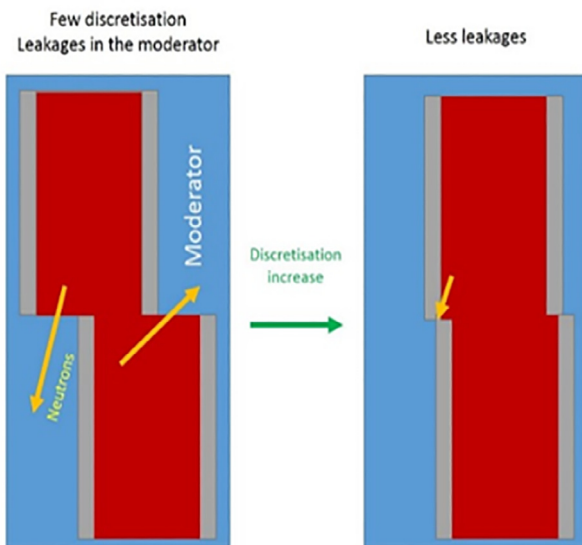


Fig. 17. Representation of high-slope sections with stacked cylinders; leaking surfaces between fuel core (in red) and moderator (in blue) ignoring the cladding (in grey).

numbers of segments appears easily feasible but worthless since they come with higher computation cost than the accurate range identified above. Fig. 16 shows simulation times (in terms of number of realizations, or batches, per second, with the higher the number, the better the computational performance). It can be observed the semi-discrete approach is more efficient than the reference for less than 71 segments, since rotated cylinders require less geometric operations than the toroidal shape to compute their interaction with neutrons.

4.3. Partial conclusion for first order rod deformation

Results in terms of deviation for production rate (in %), absorption rate (in %) and k_{eff} coefficient (in pcm) with respect to the reference for both semi-discrete approaches and the three considered deflections are gathered in Table 1. For comparison purposes, the same range of number of discrete entities is chosen for stacking and segment modeling, i.e. 30–101.

These global results confirm the observations made for the specific case of the 20-mm deflection: for similar numbers of discrete entities, segment modeling is more accurate in almost all cases.

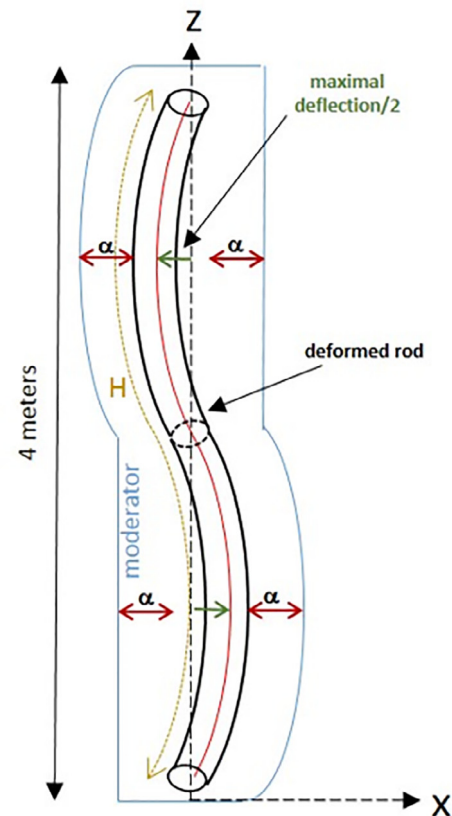


Fig. 18. Considered geometry and boundary conditions for the second order comparison case (lateral, top and bottom boundaries are set to reflection, Y-axis boundaries are set to translation).

Stacking approach shows poor accuracy when the deflection increases, which can be easily understood with the schematics in Fig. 17. Large deflections yields high slopes for the neutral fiber, especially when it crosses the initial axis of the straight rod. This tends to increase the exchange surface between the fuel and the moderator while volume of fuel and moderator are still the same using stacking modeling. This could have an impact on reactions rates.

The segment modeling should then be preferred in most cases involving dominant C-shape rod deformation and if chosen for its easier implementation, the stacking approach should be restricted to small deflections.

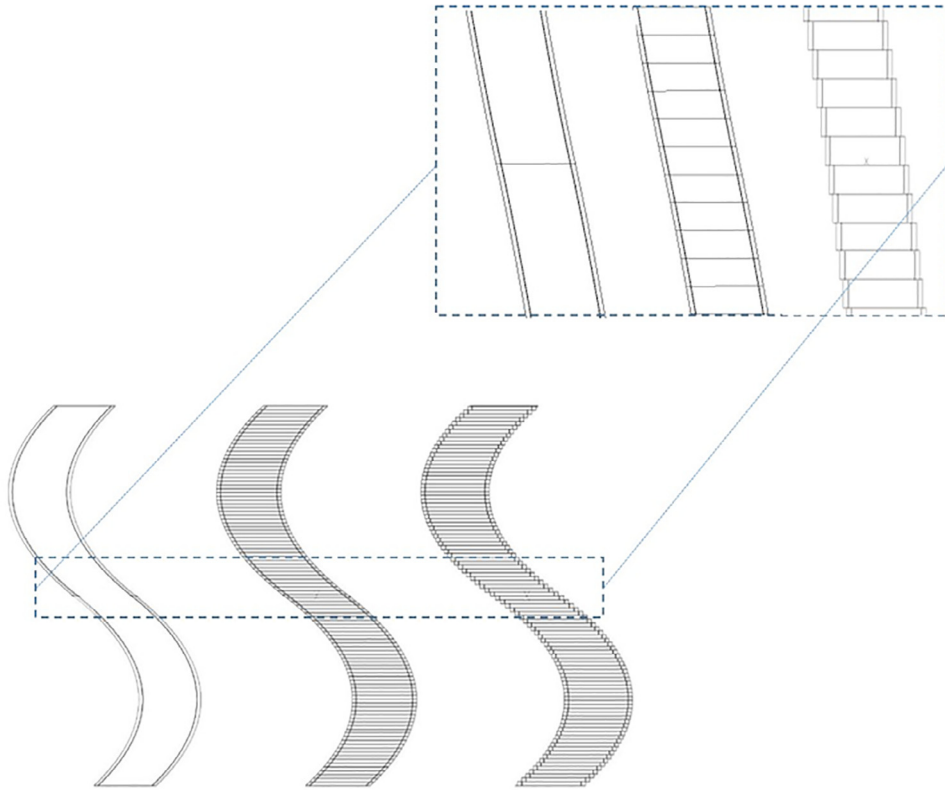
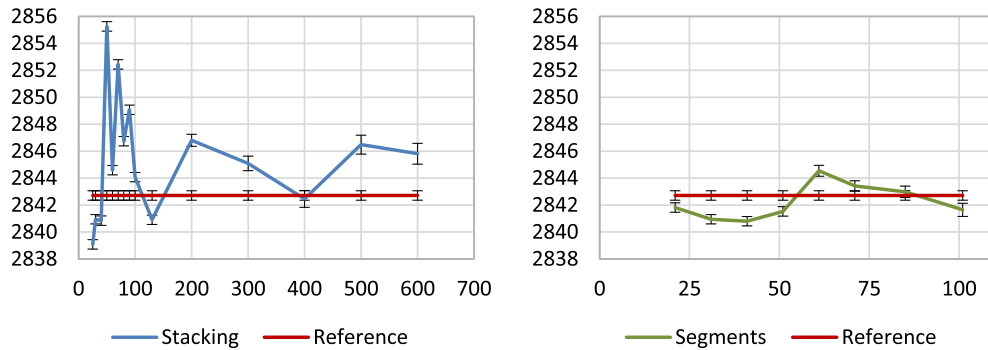


Fig. 19. Illustration of computational models second order deformation, with distinction between the inner part of the rod with fuel properties and the lateral part with cladding properties (from left to right: cut torus (reference), segments, and stacking, scales not conserved for the sake of clarity). The fuel-clad gap is too small to be observed on the figure.



(a) Production rate (s⁻¹) obtained with stacking modeling implementing 20 to 600 cylinders

(b) Production rate (s⁻¹) obtained with segment modeling implementing 21 to 101 segments

Fig. 20. Neutron production rate in U-5 for stacking and segment modeling compared to reference.

5. Compared results for second order rod deformation

Clear conclusions could be drawn after considering first order deformation in previous section. The present section aims at confronting them with the significant case for which a reference solution is fully available, in the hope of being able to design solid guidelines for generic bowing patterns of rods and assemblies.

A second order pattern is thus considered, especially introducing sections of higher slopes along the rod for the same level of deflection compared to first order deformation. The physical setup for Tripoli-4[®] is illustrated in Fig. 18 (notations are the same as before) and views of the computational models are given in Fig. 19.

The quantities of interest are the same as those in the previous section. Detailed results are given for a deflection of 10 mm for

each half of the second order bowing pattern, which yields a cumulative deflection of 20 mm along the rod, like for the first order bowing pattern above. Deflections of 10 mm and 25 mm are also considered, with results gathered in Section 5.3. The geometric correction for the segment modeling is kept from the previous section in the case of 51 segments along the rod.

5.1. Neutrons production and absorption rates

Results for neutron production in U-5 are provided in Fig. 20, whereas results for neutron absorption in U-8 are provided in Fig. 21.

The observations made in Section 4.1 still hold in the present situation, with amplified drawbacks for the stacking approach.

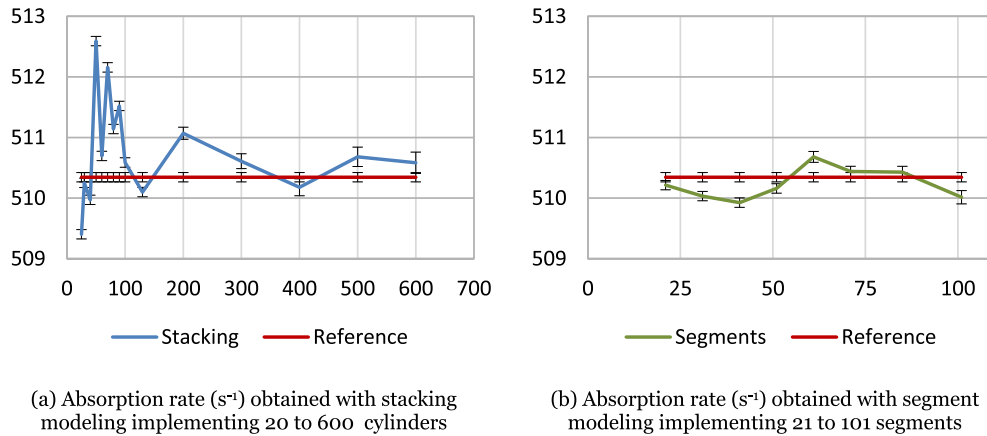


Fig. 21. Neutron absorption rate in U-8 for stacking and segment modeling compared to reference.

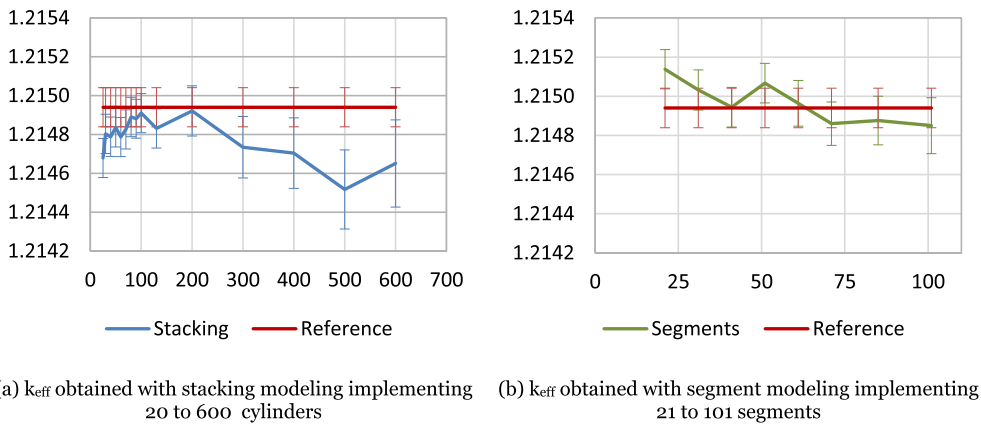


Fig. 22. k_{eff} coefficient for stacking and segment modeling compared to reference.

Table 2
Compiled results for both semi-discrete approaches and three values of deflections (10, 20 and 25 mm): deviation for production rate (in %), absorption rate (in %) and k_{eff} coefficient (in pcm). For rates: $\sigma < 0.1\%$ and for k_{eff} $\sigma < 15$ pcm.

Deflection	Segment			Stacking			
	Deviation			Deviation			
	Min	Mean	Max	Min	Mean	Max	
U5 (%)	10	0,00	0,02	0,02	0,05	0,12	0,20
	20	0,01	0,04	0,07	0,05	0,17	0,44
	25	0,04	0,13	0,33	0,01	0,14	0,35
U8 (%)	10	0,01	0,03	0,05	0,03	0,10	0,19
	20	0,02	0,05	0,08	0,02	0,17	0,44
	25	0,05	0,13	0,32	0,01	0,15	0,34
k_{eff} (pcm)	10	0,90	2,73	7,00	2,30	6,26	10,70
	20	0,40	6,87	12,70	3,00	9,99	15,30
	25	0,10	6,25	13,20	10,30	18,70	33,70

The segment modeling again yields results close to the reference and the length correction computed for 51 segments with the first order bowing pattern accurately apply in this case with the second order pattern.

5.2. Global k_{eff} coefficient

Results for both modeling are given in Fig. 22.

Observations from Section 4.2 apply again. A significant discrepancy is observed when increasing the number of stacked cylinders over 200, which can be seen as an aggravated consequence of the complex neutron leakage process through singular interfaces

between cylinders already mentioned above, since increasing the number of cylinders also increases the number of such interfaces.

5.3. Partial conclusion for second order rod deformation

Like in Section 4.3 for the first order deformation, results in terms of deviation for production rate (in %), absorption rate (in %) and k_{eff} coefficient (in pcm) with respect to the reference for both semi-discrete approaches and the three considered deflections are gathered in Table 2. The same range of numbers of discrete entities is chosen for stacking and segment modeling, i.e. 30–101.

Table 3

Main conclusions of the evaluation of stacking and segment approaches to represent first and second order bowing patterns.

Reference modeling built out of analytical shapes (torus and planes)	Semi-discrete approaches	
	Stacking modeling	Segment modeling
Easy to implement but restricted to basic bowing patterns	Easy to implement for any kind of geometry	Implementation possible for any kind of geometry with practical constraints to handle with care: length correction, priorities between entities to manage overlapping areas
Exact representation of the geometry for the suitable bowing patterns	Singular surfaces between stacked cylinders with spurious effects increasing with the bowing deflection (systematic k_{eff} underestimation observed in particular)	Fairly accurate representation of any curved geometry, assuming a relevant value for the length correction factor
Non-applicable to actual in-core deformation patterns	Accuracy and robustness for neutronics ensured only for small deflections in the case of complex bowing patterns	Recommended approach for representing actual in-core rod/assembly bowing patterns and their effect onto core neutronics

These results confirm that segment modeling should be preferred over stacking modeling, which must be restricted to very small deflections with second order deformation (a few mm).

Concerning segment modeling specifically, the accuracy of the results obtained in both configurations suggests that this approach exhibits enough regularity and robustness to be extended as expected to mixed-type generic bowing patterns.

6. About the calculations' uncertainties

A particular attention should be paid to the comparison of k_{eff} values. Even though the uncertainties are lower than 15 pcm, a majority of intervals (between models and their reference) overlap considering the 3σ -uncertainties (see Figs. 15 and 22). One has to get some distance when comparing both models with the k_{eff} coefficient.

However, regarding the reaction rates, all Tripoli-4[®]'s uncertainties order of magnitude match the ones highlighted in the different figures. The 3σ -uncertainties are way lower than 0.1 (in %), in other words, all conclusions regarding both U5 and U8 rates can be drawn without doubt.

7. Final conclusion and open prospects

The present study proposed two semi-discrete approaches to represent the effect of fuel rod/assembly bowing onto neutronics, the first based on stacked vertical cylinders to approximate the curved geometry and the second implementing rotated cylinders, named segments, instead.

Fully tested on C-shaped and S-shaped deformation patterns, both modeling can be used with a satisfactory accuracy for small deflections. However, despite specific constraints to build accurate datasets out of segments, especially related to the length correction requested to avoid gaps between consecutive segments, this latter approach produces more robust results when dealing with deflections of any shape and amplitude (see Table 3 for a full summary of the proposed evaluation).

The next step for this research is to take into account in the computational models for neutronics the local effects of rod/assembly bowing on the thermalhydraulics of the surrounding coolant. Indeed, modifications in the flow yield density modifications and then, changes in the moderation/absorption properties of water. It may also modify the local concentration of boric acid, which can result in competitive effects with measurable consequences on the reactivity of the global system.

Acknowledgements

The authors would like to thank the Tripoli-4[®] team at the CEA's SERMA unit for all the necessary support lent to this work.

References

- Andersson, T. et al., 2005. A decade of assembly bow management at Ringhals. Proceedings of a technical meeting (IAEA-TECDOC-1454).
- Brun, E., 2015. Tripoli-4[®], CEA, EDF, and AREVA reference Monte Carlo code. Ann. Nucl. Energy 82, 151–160.
- Coppolani, P., 2004. La chaudière des réacteurs à eau sous pression. EDP Sci.
- Fernandez R., EDF, 16/06/2010. Modélisation de la déformation d'assemblages combustibles dans une centrale REP, pp 12–17. Available on www.code-aster.org.
- Fetterman, R.J., 2008. Analysis of PWR assembly bow. Proceedings of International Conference on Reactor Physics (PHYSOR'08). International Conference on Reactor Physics, Nuclear Power: A Sustainable Resource.
- Gabrielsson, T., 2018. Investigation of the Development of Fuel Assembly Bow in Ringhals 3 and 4. TopFuel 2018.
- Grard, H., 2014. Physique, fonctionnement et sûreté des REP. Le réacteur en production. EDP Sciences.
- IAEA, 2008. Review of Fuel Failures in Water Cooled Reactors.
- Karlsson, L., 1999. Modeling of PWR fuel assembly deformations during irradiation. In: Structural mechanics in reactor technology, Korean Nuclear Society.
- Kepisty, G., 2016. Parametric studies of the PWR fuel assembly modeling with Monte-Carlo method. Ann. Nucl. Energy 94, 189–207.
- Kerkar, N., Paulin, P., 2008. Exploitation des cœurs REP. EDP Sci.
- Li, J., 2017a. UO₂ fuel pin bowing effects on isotopic concentrations. Ann. Nucl. Energy 105, 361–368.
- Li, J., 2017b. Bowing effects on isotopic concentrations for simplified PWR assemblies and full cores. Ann. Nucl. Energy 110, 1023–1029.
- Mukin, R., 2017. Thermal hydraulic analysis of PWR assembly bowing using subchannel code COBRA-TF. 17th International Topical Meeting on Nuclear Reactor Thermal Hydraulics (NURETH-17).
- Mukin, R., 2018. Subchannel modeling of single rod bowing in a bundle geometry. Nucl. Eng. Des. 340, 347–369.
- Patarin, L., 2002. Le cycle du combustible nucléaire. EDP Sci.
- Saeed, A., 2016. Estimation of axial and radial in-core power peaking in PWR plant using artificial neural network technique. International Conference on Emerging Technologies (ICET).
- Santamarina, A. et al., 2009. The JEFF-3.1.1 Nuclear Data Library OECD/NEA JEFF Report 22. Organisation for Economic Co-operation and Development/Nuclear Energy Agency.
- Konheiser, J. et al., 2016. Investigation of the effects of a variation of fuel assembly position on the ex-core neutron flux detection in a PWR. Journal of Nuclear Science and Technology.
- SERPENT – a Continuous-energy Monte Carlo Reactor Physics Burnup Calculation Code, (2015) User's manual, J. Leppänen, VTT, Finland, montecarlo.vtt.fi.
- Shishkov, L., 2015. Inter-assembly gap deviations in VVER-1000: Accounting for effects on engineering margin factors. Kerntechnik 80, 408–411.
- Syrjälähti, E., 2019. Modeling burnup-induced fuel rod deformations and their effect on transient behavior of a VVER-440 reactor core. Ann. Nucl. Energy 125, 121–131.
- Wanninger, A., 2018. Mechanical analysis of the bow deformation of a row of fuel assemblies in a PWR core. Nucl. Eng. Technol. 50, 297–305.